actuators

Article

Multi-Objective Cooperative Adaptive Cruise Control Platooning of Intelligent Connected Commercial Vehicles in Event-Triggered Conditions

Jiayan Wen [1,2], Lun Li [1,2], Qiqi Wu [1,*], Kene Li [1,2] and Jingjing Lu [1]

[1] School of Automation, Guangxi University of Science and Technology, Liuzhou 545616, China; wenjyan@gxust.edu.cn (J.W.); 20220203034@stdmail.gxust.edu.cn (L.L.); likene@gxust.edu.cn (K.L.); 100002395@gxust.edu.cn (J.L.)

[2] Research Center for Intelligent Cooperation and Cross-Application, Guangxi University of Science and Technology, Liuzhou 545616, China

* Correspondence: 100000327@gxust.edu.cn

Abstract: With the rapid increase in vehicle ownership and increasingly stringent emission regulations, addressing the energy consumption of and emissions from commercial vehicles have become critical challenges. This study introduces a multi-objective cooperative adaptive cruise control (CACC) strategy, designed for intelligent connected commercial vehicle platoons, operating in event-triggered conditions. A hierarchical control framework is utilized: the upper layer handles reference speed planning based on vehicle dynamics and constraints, while the lower layer uses distributed model predictive control (DMPC) to manage vehicle following. DMPC is chosen for its ability to manage distributed platoons by enabling vehicles to make local decisions, while maintaining system-wide coordination. Additionally, adaptive particle swarm optimization (APSO) is employed during the optimization process to solve the optimal problem efficiently. APSO is employed for its computational efficiency and adaptability, ensuring quick convergence to optimal solutions with reduced overheads. An event-triggering mechanism is integrated to further reduce the computational demands. The simulation results show that the proposed approach reduces fuel consumption by 8.05% and NO_x emissions by 10.15%, while ensuring stable platoon operation during dynamic driving conditions. The effectiveness of the control strategy is validated through extensive simulations, highlighting superior performance compared to conventional methods.

Keywords: CACC; distributed model predictive control; fuel consumption optimization; NO_x emissions; adaptive particle swarm optimization; event-triggered conditions

Citation: Wen, J.; Li, L.; Wu, Q.; Li, K.; Lu, J. Multi-Objective Cooperative Adaptive Cruise Control Platooning of Intelligent Connected Commercial Vehicles in Event-Triggered Conditions. *Actuators* **2024**, *13*, 522. https://doi.org/10.3390/act13120522

Academic Editor: Anyang Lu

Received: 5 November 2024
Revised: 10 December 2024
Accepted: 16 December 2024
Published: 17 December 2024

1. Introduction

With the development of the economy and transportation, the number of commercial vehicles for long-distance transportation is increasing strongly, year by year. Due to the rapid increase in commercial vehicles, environmental pollution and energy consumption are becoming increasingly serious. It is of great theoretical and commercial value to research how to effectively reduce vehicle fuel consumption and emissions. Currently, the rapid development of intelligent transportation systems (ITSs) provides a theoretical basis for vehicle-to-infrastructure (V2I) cooperation and vehicle-to-vehicle (V2V) cooperation. If commercial vehicles on the road are combined and controlled as a whole, traffic congestion can be alleviated, road throughput can be improved, and energy consumption [1] and the average wait time can be reduced [2]. From the perspective of control, a platoon can be divided into four interrelated parts: (1) node dynamics, (2) information flow topology, (3) formation geometry, and (4) the distributed controller [3]. This paper mainly studies vehicle operation optimization from the perspective of control. As node dynamics and information flow topology are not involved in control, they are not included here.

To address the formation geometry problem, Zheng [4] studied a time-varying formation control algorithm based on an unmanned intelligent vehicle (UIV) system. Building on this, a formation algorithm utilizing consistency theory was proposed for use when the formation reference center moves and multiple time-varying formations within the multi-agent system were achieved through simulations. The simulation results demonstrated that the proposed algorithm effectively and quickly adjusts to different formation requirements, with a strong performance in terms of control effectiveness and robustness. In vehicle platooning, the behavior of each vehicle is influenced by the others, so single-vehicle optimization metrics cannot be applied to optimize the entire platoon. Game theory has been introduced as a method to achieve stability by facilitating a continuous game between individual vehicles in the formation, leading to optimal results for the entire platoon. Jond et al. [5] employed the differential game method to establish a mathematical model for vehicle formation control, proving the existence of the Nash equilibrium controller for connected automated vehicles (CAVs), which was used to manage vehicle formations. In transportation tasks, commercial vehicles often face constraints related to distance and time. Wang et al. [6] proposed a spatiotemporal synchronous control method that separates and independently controls time and space by associating and decoupling the reference and actual kinematics of the vehicle and the target in a polar coordinate system. This method allows for synchronous tracking and formation, where the system reaches a predetermined state with a fixed relative spatial trajectory at a specified terminal time, enabling simultaneous tracking and formation of multiple vehicles.

In terms of distributed controllers for platoon control, He et al. [7] proposed a new distributed economic model predictive control (EMPC) method to address platoon optimization problems with nonlinear dynamics and safety constraints. This EMPC method ensures stable operation of the platoon, while improving fuel economy. Mihaly et al. [8] developed a decentralized model predictive control framework for vehicle coordination at intersections, predicting the time of arrival and using linear constraints to avoid collisions. The simulation results from various scenarios show that this method not only guarantees near-optimal solutions within a decentralized framework, but also has the potential for real-time implementation in regard to urban traffic. Li et al. [9] introduced a control strategy for fuel cell electric vehicles, which integrates top-level centralized and bottom-level distributed controllers. This strategy utilizes eco-driving CACC and the Equivalent Consumption Minimization Strategy (ECMS) to generate optimal control inputs, enhancing the energy-saving potential and stability, thereby improving the platoon's following performance and energy efficiency. Wen et al. [10] proposed a practical platoon control algorithm, designing a feedback controller based on a connected state matrix. This algorithm ensures both platoon stability and zero steady-state spatial error in regard to the gain of each controller.

In the design of distributed controllers, while abundant network information can enhance system stability, it also imposes a substantial computational burden. Therefore, it is necessary to explore platoon stability control using reduced information transmission.

Event-triggered control is an effective solution for mitigating communication delays and reducing computational overheads by triggering control updates based on system state errors. Zhang et al. [11] presents a method for ensuring stability with reduced sampling frequency by triggering events based on accumulated state errors. Accumulative-error-based event-triggered control for discrete-time linear systems improves system efficiency by using error thresholds to minimize unnecessary updates [12]. Additionally, event-triggered output feedback synchronization for master–slave neural networks has been explored, showing resilience to deception attacks [13]. Wen et al. [14] developed a dynamic event-triggered communication mechanism (DECM), which significantly reduces the transmission of the leading vehicle's sampled speed and acceleration. The simulation results demonstrate that a DECM-based CACC system not only conserves communication resources within the platoon, but also ensures stable performance. He et al. [15] theoretically analyzed the impact of lead vehicle information on platoon dynamics, proving that the lead vehicle's data can overshadow the effects of other vehicles. Based on this finding, the interaction topology of the platoon can be designed as a tree structure rooted in the lead vehicle, with the lead vehicle only needing to communicate with nearby vehicles to reduce the burden of information flow [16]. Wen et al. [17] developed a decentralized event-triggered control strategy for multi-agent systems, effectively reducing the communication load and ensuring stability, even with network-induced delays.

In regard to platoon cruise control, uncertainties in the state of the lead vehicle, unknown external disturbances, and communication delays often introduce negative impacts. To address these issues, Massera et al. [18] proposed a robust optimal control method based on the minimum safe distance between vehicles, providing a theoretical lower limit for safe distances and accounting for disturbances caused by vehicle acceleration. Guo et al. [19] combined integral sliding mode technology with adaptive neural networks to achieve optimal control of a platoon in situations involving unmodeled nonlinear dynamics, unknown disturbances, and input saturation. Zhu et al. [20] developed an event-triggered mechanism based on platoon formation errors and designed a distributed data-driven controller to accomplish platoon control tasks. Their proposed fault-tolerant distributed event-triggered control method ensured safe platoon control, even when partial sensor failures occurred. Feng et al. [21] proposed a nonlinear heterogeneous automated vehicle (AV) coordination control algorithm, which addresses uncertain interaction topologies, parameter errors, and external disturbances, simultaneously. Gao et al. [22] studied vehicle tracking control involving model parameter uncertainties and external disturbances, proposing a new fixed-time backstepping control scheme to ensure that the vehicle follows a predefined trajectory and guarantees global fixed-time stability of the closed-loop system. Liu et al. [23] proposes an adaptive control method for vehicular platoons in the presence of time-varying actuator faults and distance constraints. A novel Nussbaum function is designed to address unknown fault directions and a Barrier Lyapunov Function (BLF) technique is employed to handle asymmetric distance constraints. The control strategy ensures both individual vehicle stability and string stability within a fixed time frame. The simulation results demonstrate the method's effectiveness, confirming its ability to maintain system stability and collision avoidance, even under the impact of actuator faults and external disturbances. Moreover, recent research has highlighted the critical role of road friction in vehicle platooning control. Santini et al. [24] proposed a real-time road friction estimation technique that combines a bicycle vehicle model with a tire Magic Formula approach, enabling adaptive inter-vehicle spacing adjustments based on varying road conditions, such as wet or icy surfaces. This method has been validated in autonomous driving scenarios, demonstrating its effectiveness in maintaining safety and preventing collisions in adverse environments. Similarly, Zuo et al. [25] formulated a road friction-based spacing policy to improve platoon safety by integrating road friction coefficients into a safety cost function. This approach allows automatic adjustments of inter-vehicle spacing based on road friction, ensuring stability and optimizing safety for nonlinear vehicle platoons.

Evolving intelligent connected vehicles (ICVs) present new complexities, particularly in mixed traffic, where communication delays and vehicle diversity complicate control. While intelligent solutions offer promising approaches to these challenges, they often rely on reliable communication and accurate sensors, making them vulnerable to delays and uncertainties. Additionally, their computational demands can hinder scalability in large-scale platoons or resource-limited environments. Wang et al. [26] proposed a Deep-LCC (Data-Driven Predictive Leader–Follower Cruise Control) method to address challenges in mixed traffic scenarios. Ma et al. [27] focused on the issue of large ICV platoon splitting into sub-platoons due to communication limitations. They extended various car-following models using the Intelligent Driver Model (IDM) and proposed an adaptive gain feedback control strategy to enhance anti-interference capabilities in mixed traffic. Huang et al. [28] explored ICV platoon control involving acceleration constraints, using robust model predictive control. Qiu et al. [29] investigated platoon control on curved paths, using a sliding mode control framework and proving asymptotic convergence using Lyapunov methods, with numerical simulations confirming the controller's effectiveness. Min et al. [30] proposed a merging strategy for vehicle platoons, considering the safety space and acceleration limits of two adjacent platoons consisting of connected and automated vehicles. They validated their approach through simulations across different scenarios. Shi et al. [31] addressed the control of vehicle platoons and individual ICVs at highway ramp junctions in mixed traffic flows. They proposed an optimal control strategy based on Pontryagin's Minimum Principle (PMP), with flexible merging points, and numerical simulations demonstrated significant improvements in overall traffic throughput.

The current research has two primary limitations: first, most studies focus solely on vehicle dynamics optimization without considering fuel consumption, emissions, and power limitations of the underlying engine system. This results in optimization methods that cannot effectively balance fuel consumption and NO_x emissions. Second, in solving the cruise control optimization problem, direct numerical solutions struggle to meet the real-time computing demands of embedded systems, while indirect methods tend to fall into the category of local optima, reducing control performance.

To comprehensively optimize vehicle fuel consumption and NO_x emissions, this paper proposes an optimal cruise control method based on distributed model predictive control (DMPC). DMPC is chosen for its ability to handle the distributed nature of vehicle platoons, where each vehicle can make decisions based on local information, while maintaining overall system performance. The contributions of this research are as follows:

1. At the vehicle level, engine fuel consumption and NO_x emission characteristics are incorporated, establishing models related to vehicle speed and acceleration;
2. Vehicle state constraints are formulated in combination with engine power limitations to ensure the feasibility of the optimization results and a cruise optimization problem that considers both fuel consumption and NO_x emissions is constructed;
3. In regard to controller design, an error-based event-triggered mechanism is developed to reduce the computational resources needed and APSO is employed to optimize the control inputs, improving system convergence performance. APSO is chosen for its ability to avoid the complex computations required in terms of traditional iterative methods. Additionally, APSO's adaptability ensures quick convergence to an optimal solution, with less computational overheads.

The remainder of this paper is organized as follows. Section 2 introduces the control-oriented model. Section 3 details the construction of the vehicle's optimal controller. The simulation results and discussion are provided in Section 4. Finally, the conclusions are presented in Section 5.

2. Establishing a Control-Oriented Model

2.1. Vehicle Dynamics Model

This paper focuses on intelligent connected commercial vehicles equipped with a vehicle body module, diesel engine module, and after-treatment system. The driving scenario is limited to flat road surfaces, defined as idealized conditions without obstacles or lateral irregularities. However, longitudinal grades are incorporated to account for grade resistance, enhancing the model's applicability to real-world driving conditions. The relationship between the motion of two adjacent vehicles in a platoon is depicted in Figure 1.

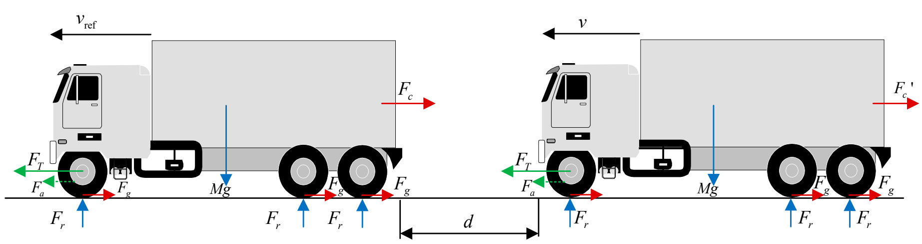

Figure 1. Schematic diagram of adaptive cruise control.

Based on the balance of the vehicle's driving force and resistance during motion, the longitudinal dynamics model of the lead vehicle is derived as follows:

$$F_T = F_c + F_r + F_g + F_a, \quad (1)$$

In this equation, F_T represents the vehicle's traction force, F_c denotes the aerodynamic drag, F_r is the rolling resistance, F_g is the grade resistance, and F_a is the effective driving force, which is defined as the net force after subtracting all the resistances from the traction force. The equation is expressed as:

$$\frac{\eta T_e}{r} = \frac{\rho C_d A_F}{2} v^2 + Mg\sin(\theta) + MgC_g\cos(\theta) + Ma, \quad (2)$$

where η is the transmission efficiency, T_e is the engine's output torque, r is the tire radius, ρ is the air density, A_F is the frontal area of the vehicle, C_d is the aerodynamic drag coefficient, v is the vehicle velocity, M is the vehicle mass, g is the gravitational acceleration, θ is the road gradient, C_g is the rolling resistance coefficient, and a is the vehicle's acceleration. Based on [32], the aerodynamic drag coefficient C_d changes with the distance between the subject vehicle and the preceding vehicle, and its detailed expression is given by the following equation:

$$C_d = C_0\left(1 - \frac{C_1}{C_2 + d}\right), \quad (3)$$

In the equation, C_0 represents the aerodynamic drag coefficient in the absence of any preceding vehicle, $C_1 = 1.875$ and $C_2 = 0.0298$ are constants obtained through data fitting, and d denotes the relative distance between the vehicles. Based on the vehicle dynamics model, the longitudinal dynamics of the vehicle can be further described as:

$$Ma = F_T - F_c - F_r - F_g. \quad (4)$$

2.2. Fuel Consumption and NO_x Emission Model

Due to the nonlinear trade-off relationship between fuel consumption and NO_x emissions in commercial diesel vehicles, to better describe the instantaneous relationship between the two, this paper introduces an energy equivalent fuel consumption model into the controller design of the optimization problem:

$$F_R(k) = \frac{1}{2} p_1 M v(k)^2, \quad (5)$$

where p_1 represents the efficiency of converting thermal energy from diesel combustion into kinetic energy, with specific values obtained through parameter fitting. Based on the literature [33,34], the NO_x emission model is established using vehicle speed and acceleration as input variables. The least squares method is employed for fitting the target function, where the fitting process uses a square loss function, minimizing the sum of the squared errors to identify the optimal fitting model. The New European Driving Cycle (NEDC) and China Heavy-duty Truck Cycle (CHTC-H) data, including vehicle speed and corresponding fuel consumption and emission data, are selected as training datasets for model training and iterative optimization.

$$E_N(k) = q_{0,0} + q_{1,0}a(k) + q_{0,1}v(k) + q_{2,0}a(k)^2 + q_{1,1}a(k)v(k), \quad (6)$$

where $q_{0,0}$, $q_{1,0}$, $q_{0,1}$, $q_{2,0}$, and $q_{1,1}$ are parameters obtained through fitting and their specific values are shown in Table 1.

Table 1. Parameters of the fuel consumption and NO_x emission model.

Parameter	Value	Unit
p_1	6.358×10^{-6}	-
$q_{0,0}$	0.0406	-
$q_{1,0}$	0.01063	-
$q_{0,1}$	0.03735	-
$q_{2,0}$	−0.001085	-
$q_{1,1}$	0.01124	-

3. Construction of the Vehicle's Optimal Controller

The optimal control of commercial vehicles for long-distance transportation on highways can be divided into platoon formation optimization and platoon operation optimization. This paper optimizes the cruise control of vehicle platoons during long-distance transportation on highways. A general view of the overall research is shown in Figure 2. To simplify the problem, it is reasonable to consider that the platoon is homogeneous. In Figure 2, the destination distance s_f, road slope θ, road speed limit and other information can be obtained through V2I and V2V, which can be used to plan the cruise speed $v_{i,\mathrm{ref}}$. The reference speed $v_{i,\mathrm{ref}}$ is communicated to the inner platoon vehicles via V2V. These vehicles are tasked with tracking the $v_{i,\mathrm{ref}}$. However, due to information transmission delays, speed tracking errors, and other influencing factors, the actual speed and acceleration of each vehicle are represented as v_i and a_i, respectively.

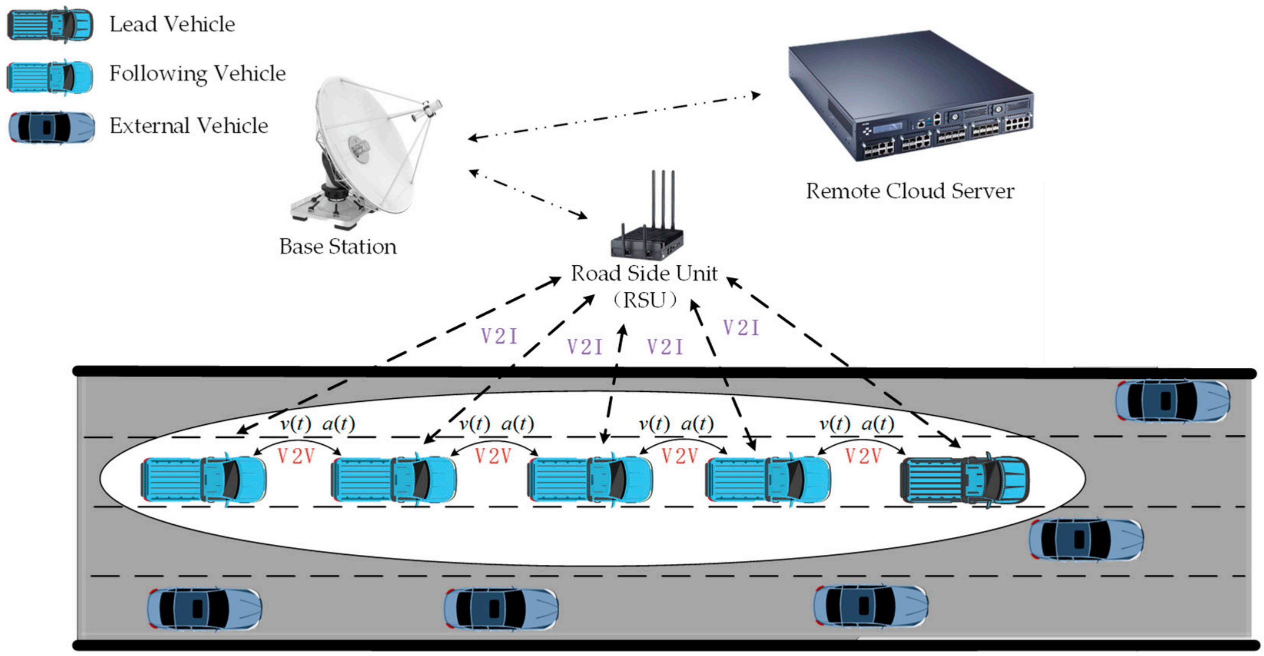

Figure 2. Schematic diagram of CACC platoon for intelligent connected commercial vehicles.

3.1. Reference Speed Planning

After solving the vehicle control inputs, it is necessary to convert the constrained optimization problem, which coordinates the vehicle's fuel consumption and emissions, into an unconstrained problem. Typically, the obstacle function method is employed to incorporate inequality constraints into the objective function. However, both exponential and logarithmic obstacle functions introduce significant nonlinearity, which not only increases the computational complexity, but also complicates hardware implementation. Therefore, this paper adopts a hierarchical optimization strategy. First, the reference speed of the controlled vehicles in the platoon is determined by considering the constraints, such as the speed of the leading vehicle and traffic flow conditions. Then, speed tracking control is applied to each vehicle.

During the planning of the lead vehicle's speed, it is unnecessary to consider the safety constraints of the following vehicles. The lead vehicle only needs to set an appropriate cruising speed based on the time requirements of the transportation task and the driver's preferences, within the bounds of the road's speed limits. Since the determination of the lead vehicle's reference speed is relatively straightforward, it is not discussed further in this paper. Instead, the focus is on how to plan the reference speed for other individual vehicles in the platoon, after the lead vehicle's cruising speed has been established.

To ensure the safe operation of vehicles, speed and distance limits must be imposed. As the method proposed in this paper optimizes the instantaneous behavior of vehicles, the safety distance constraint can be equivalently translated into a safe speed constraint, providing real-time vehicle safety speed restrictions. Using V2X technology, vehicles can obtain the speed information of the preceding vehicle and calculate a safe speed constraint based on their current state. The speed limits $v_{i,\max}(t)$ are as follows [35]:

$$v_{i,\max}(t) = \min\{v_{i,\max1}(t), v_{i,\max2}(t), v_{i,\max3}(t), v_{i,\max4}(t)\}. \tag{7}$$

where $v_{i,\max1}(t)$ represents the maximum speed limit of the road, which in this paper is set to 33 m/s; $v_{i,\max2}(t)$ represents the speed that maintains a safe distance from the preceding vehicle, expressed as:

$$v_{i,\max2}(t) = \frac{s_{i-1}(t) - s_i(t) - v_i(t)\tau}{T_{i,\text{react}}}. \tag{8}$$

where $s_{i-1}(t)$ is the distance of the (i − 1)th vehicle, $s_i(t)$ is the distance of the ith vehicle, τ is the sampling time, and $T_{i,\text{react}}$ is the driver's emergency response time. Moreover, $v_{i,\max3}(t)$ is the safety speed constraint of the vehicle during emergency braking, which is in the form of:

$$v_{i,\max3}(t) = -a_{i,b,\max}T_{i,\text{react}} + \sqrt{a_{i,b,\max}^2 T_{i,\text{react}}^2 + 2a_{i,b,\max}c(t) + \frac{a_{i,b,\max}}{a_{i-1,b,\max}}v_{i-1}^2(t)}. \tag{9}$$

where $a_{i,b,\max}$ is the maximum deceleration of the vehicle during braking and $a_{i-1,b,\max}$ represents the maximum deceleration of the preceding (i − 1)th vehicle, which can be obtained via V2X communication. In this paper, the maximum deceleration is set to 3.5 m/s^2. Define $c(t) = s_{i-1}(t) - s_i(t) - v_i(t)\tau$, where $v_{i,\max4}(t)$ is the vehicle's maximum speed constrained by its dynamic system, which can be expressed as:

$$v_{i,\max4}(t) = \frac{F_T\tau}{M}. \tag{10}$$

Since vehicles on highways must comply with legal speed limits, the minimum speed limit, $v_{i,\min}$, is set to 22 m/s. The final reference speed is constrained as follows:

$$v_{\text{i,ref}} \in [v_{i,\min}, v_{i,\max}]. \tag{11}$$

3.2. Constructing the Objective Function

In the development of objective functions, prior studies have predominantly employed vehicle kinetic energy as a measure of energy consumption [36]. Moreover, most of this research has concentrated on optimizing a single objective, either fuel consumption or emissions [37,38], without considering the trade-off between these two factors. To enable balanced optimization of both fuel consumption and NO_x emissions for platoons cruising on highways, this paper formulates the objective function by combining Equations (5) and (6), which account for fuel consumption and NO_x emission performance:

$$J_i = \int_{t_0}^{t_0+N_p} \Big(\omega_f F_R(t) + \omega_e E_N(t) + \omega_a a_i(t)^2 + \omega_v (v_i(t) - v_{i,ref}(t))^2\Big)dt, \tag{12}$$

where N_p is the prediction horizon's end time; $(v_i(t) - v_{i,ref}(t))^2$ represents the speed tracking error term; ω_f, ω_e, ω_a, and ω_v are the weight coefficients corresponding to fuel consumption, NO_x emissions, ride comfort smoothness, and speed tracking error, respectively.

In this study, the weight coefficients were set as follows: $\omega_f = 0.5$, $\omega_f = 0.5$, $\omega_a = 1$, and $\omega_v = 10$. Equal weights for ω_f and ω_e were selected to address the inherent trade-off between these objectives, as outlined in [39], ensuring a balanced optimization approach that avoids disproportionately favoring one aspect at the expense of the other. The weight assigned to ride comfort smoothness, ω_a, reflects its moderate priority, aiming to mitigate abrupt acceleration changes and enhance driving comfort without undermining the primary optimization goals. A significantly higher weight for speed tracking error, ω_v, was adopted to emphasize its pivotal role in maintaining platoon stability and synchronization, which are critical for the safe and efficient operation of vehicle platoons. The selected weight coefficients were validated through extensive simulation experiments, confirming their efficacy in achieving well-balanced optimization across diverse operating scenarios.

3.3. Obtaining Control Constraints

Since the vehicle's acceleration depends on the dynamic performance of the powertrain, to ensure that the powertrain meets the vehicle's power demands, the specific expression for the maximum acceleration of the i-th vehicle is derived by combining Equations (2) and (4):

$$a_{i,\max}(t) = \frac{\eta_i T_{e,i,\max}(t)}{r_i M_i} - \frac{\rho C_d A_F}{2} v^2 - g\sin(\theta) - gC_{i,g}\cos(\theta). \tag{13}$$

Combined with the maximum braking acceleration $a_{i,\min}(t)$ provided by the vehicle braking system, the acceleration restriction of the vehicle is:

$$a_i(t) \in [a_{i,\min}(t), a_{i,\max}(t)]. \tag{14}$$

Briefly, the nonlinear platoon formation optimization problem can be constructed as follows:

$$\begin{aligned} &\min J_i = \int_{t_0}^{t_0+N_p} \Big(\omega_f F_R(t) + \omega_e E_N(t) + \ \omega_a a_i(t)^2 + \omega_v (v_i(t) - v_{i,ref}(t))^2\Big) dt, \\ &s.t. \quad \dot{v}_i(t) = a_i(t) - \widetilde{a}_{i,a}(t) - a_{i,r}(t) - a_{i,g}(t) \\ &\qquad\quad a_i(t) \in [a_{i,\min}(t), a_{i,\max}(t)]. \end{aligned} \tag{15}$$

3.4. Design of the Bottom-Level Distributed Model Predictive Controller (DMPC)

To address the optimization problem discussed above, this section presents a distributed model predictive control (DMPC) strategy that incorporates an event-triggered mechanism. The proposed controller provides an independent distributed control strategy for each vehicle within the platoon. To improve the computational efficiency and accuracy of the optimization process, the adaptive particle swarm optimization (APSO) algorithm is utilized to solve the optimization problem. The control inputs are determined in real time through Receding Horizon Optimization (RHO), ensuring that the system achieves multi-objective performance optimization, even in complex and dynamic conditions.

Figure 3 illustrates the overall strategy framework for cooperative adaptive cruise control (CACC) within the vehicle platoon. This framework demonstrates how upper-level speed planning and bottom-level vehicle control work together to ensure the efficient, synchronized, and safe operation of the platoon. The diagram highlights the role of the DMPC and APSO algorithms in optimizing vehicle performance, reducing fuel consumption and emissions, while the V2X communication system ensures that the vehicles remain coordinated and responsive to dynamic driving conditions and road environments.

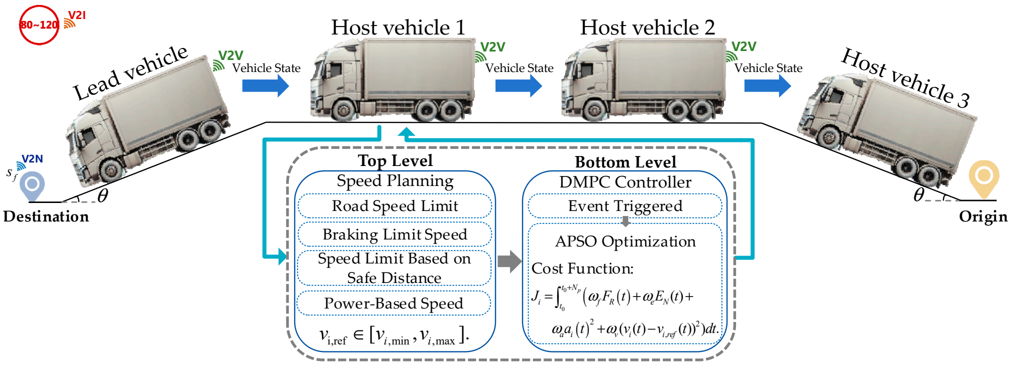

Figure 3. The overall diagram of the vehicle platoon CACC strategy.

3.4.1. DMPC Control in Event-Triggered Conditions

In this paper, the event-triggered mechanism is based on the vehicle's speed and acceleration errors. When the deviation between the current speed or acceleration and the predicted value exceeds a predetermined threshold, the controller is triggered to recalculate and update the control inputs. This mechanism continuously monitors critical state variables in real time, ensuring that optimization computations are only performed when necessary. As a result, it enhances the efficiency of computational resource utilization, while maintaining system control performance. The speed error is given by:

$$|v - v_{\text{pre}}| > \varepsilon_v, \tag{16}$$

The acceleration error is defined as:

$$|a - a_{\text{pre}}| > \varepsilon_a. \tag{17}$$

The speed error $v - v_{\text{pre}}$ satisfies (16) and the acceleration error $a - a_{\text{pre}}$ satisfies (17), where ε_v and ε_a are the speed and acceleration error thresholds, respectively. When either of the triggering conditions is satisfied, the controller executes the optimization calculation to update the control inputs.

Once the event is triggered, the MPC controller predicts the system's behavior for the next N_p steps based on the vehicle's current state and determines the optimal control inputs by solving the corresponding optimization problem. The control objective is to minimize the cost function (Equation (15)) to enhance the overall system performance. In this study, the prediction horizon N_p is set to 10.

The controller utilizes the RHO approach to dynamically adjust the control strategy, aiming to obtain the optimal control input sequence within the prediction horizon:

$$U = \{a_p(t), a_p(t+1), \ldots, a_p(t+N_p-1)\}. \tag{18}$$

where $a_p(t)$ represents the control input (acceleration) at each time step. Finally, the first control output, $a_p(t)$, from the sequence is selected as the actual control input at the current time and is applied to the system. As the system's state evolves, the MPC recalculates the control output sequence at each time step to achieve dynamic optimization within the receding horizon. This approach ensures that the system can effectively respond to changes in both the internal states and external environments, thereby maintaining stability and control performance.

3.4.2. APSO Optimization Problem Solving

For the optimization of vehicle fuel consumption and NO_x emissions, the objective function is often nonlinear and non-convex. In such cases, although traditional Sequential Quadratic Programming (SQP) methods are precise, they typically require significant computational resources and time due to their complex iterative processes and high computational complexity. To address this challenge, heuristic algorithms can provide near-optimal solutions within an acceptable computation time through the use of probabilistic search methods.

This paper employs the adaptive particle swarm optimization (APSO) algorithm to solve the problem. Compared to gradient-based methods, which require the objective function to be smooth and differentiable, this condition is not always met when handling complex nonlinear optimization problems. In contrast to other heuristic algorithms, APSO typically converges faster, as its search process is more direct and it can effectively adapt to the search space dynamics. Compared to traditional particle swarm optimization (PSO), APSO features dynamic adjustment capabilities, allowing it to adaptively switch between global and local search modes. This adaptability enhances the solution efficiency and convergence speed. The steps involved in the APSO algorithm are as follows:

Step 1. Initialize every particle parameter. The number of particles is set to N, with each particle's position and velocity represented by vectors $x_i(t)$ and $v_{l,i}(t)$, respectively, where $i = 1, 2, \ldots, N$ represents the number of particles and t represents the iteration step. The position of the particles is initialized randomly as:

$$x_i(0) = x_{\min} + (x_{\max} - x_{\min}) \cdot \mathrm{rand}(N), i = 1, 2, \ldots, N \tag{19}$$

where $x_{\min}$ and $x_{\max}$ represent the lower and upper bounds of the search space.

Step 2. The fitness calculation. Each particle's position is evaluated in regard to the objective function $J(x_i(t))$ to compute its fitness. The current fitness is compared with the particle's historical best fitness, and the individual best position $p_i(t)$ is updated as follows:

$$p_i(t+1) = \begin{cases} x_i(t),\ J(x_i(t)) < J(p_i(t)) \\ p_i(t),\ \text{otherwise} \end{cases} \tag{20}$$

Simultaneously, the global best position $g(t)$, representing the position with the best fitness among all the particles, is updated as follows:

$$g(t+1) = \min(J(p_1(t), J(p_2(t)), \ldots, J(p_N(t))). \tag{21}$$

Step 3. Inertia weight and coefficient dynamic adjustment. During the optimization process, the inertia weight $\omega(t)$, cognitive coefficient δ_1, and social coefficient δ_2 are dynamically adjusted with each iteration. This ensures a smooth transition from a global search to a local search. The update rule for the inertia weight is given by:

$$\omega(t) = \omega_{\min} + (\omega_{\max} - \omega_{\min}) \cdot \frac{t_{\max} - t}{t_{\max}}, \tag{22}$$

where $\omega_{\max}$ is the initial inertia weight, $\omega_{\min}$ is the minimum inertia weight, t is the current iteration number, and $t_{\max}$ is the maximum number of iterations. The dynamic adjustment formulas for the cognitive coefficient δ_1 and social coefficient δ_2 are as follows:

$$\delta_1(t) = \delta_1^{\max} - (\delta_1^{\max} - \delta_1^{\min}) \cdot \frac{t}{t_{\max}}, \tag{23}$$

$$\delta_2(t) = \delta_2^{\max} - (\delta_2^{\max} - \delta_2^{\min}) \cdot \frac{t}{t_{\max}}. \tag{24}$$

where $\delta_1^{\max}$, $\delta_1^{\min}$, $\delta_2^{\max}$, and $\delta_2^{\min}$ represent the initial and minimum values of the cognitive and social coefficients, respectively.

Step 4. Particle parameter update. Based on the inertia weight, individual best position, and global best position, the velocity and position of the particles are updated. The velocity update formula is as follows:

$$v_{l,i}(t+1) = \omega(t) \cdot v_{l,i}(t) + \delta_1(t)\lambda(p_i(t) - x_i(t)) + \delta_2(t)\lambda(g(t) - x_i(t)), \tag{25}$$

where λ is a random number within the range [0, 1]. The position update formula is given by:

$$x_i(t+1) = x_i(t) + v_{l,i}(t+1). \tag{26}$$

Step 5. Update individual and global best positions. Update the particle's individual best position $p_i(t)$ as follows:

$$p_i(t+1) = \begin{cases} x_i(t+1), \ f(x_i(t+1)) < f(p_i(t)) \\ p_i(t), \quad \text{otherwise} \end{cases} \tag{27}$$

Update the global best position $g(t)$ as follows:

$$g(t+1) = \text{argmin}\{f(p_1(t+1)), f(p_2(t+1)), \ldots, f(p_N(t+1))\}. \tag{28}$$

Step 6. The termination condition. Return to Step 2. The algorithm terminates and outputs the global best solution when the maximum number of iterations is reached or when the change in the global best position satisfies the stopping criterion. A detailed algorithm flowchart is shown in Figure 4.

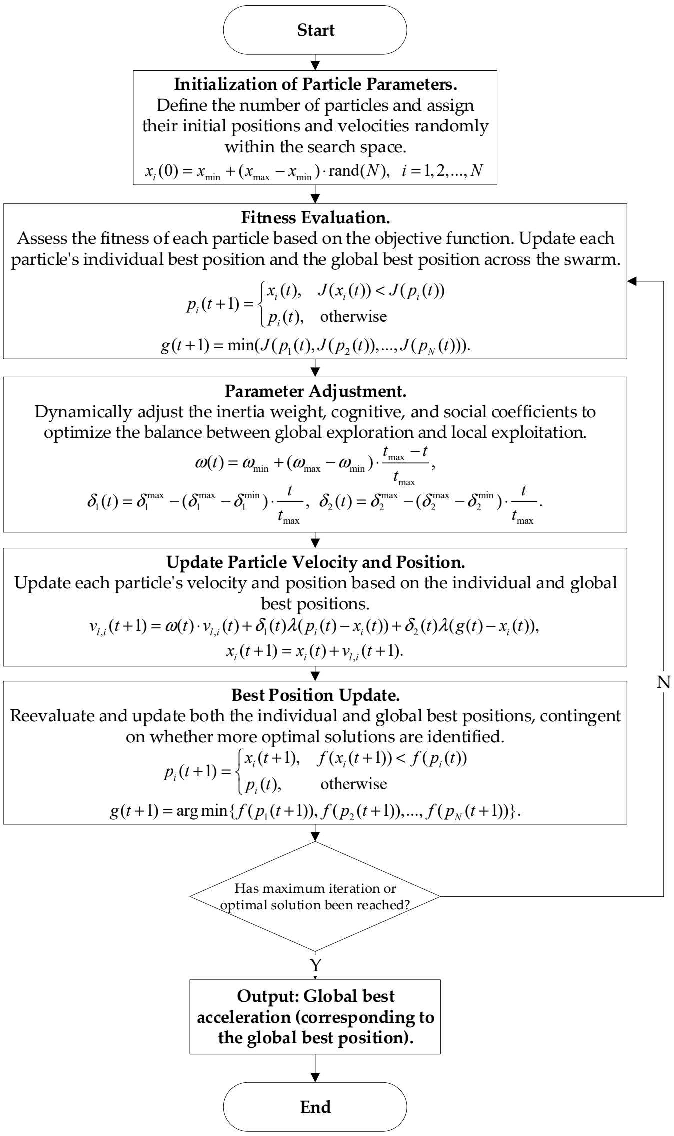

Figure 4. Flowchart of APSO algorithm.

3.4.3. System Stability Analysis

To ensure the stability of each vehicle within the platoon when using the distributed control approach, it is essential to analyze how the speed error and acceleration influence the dynamics of individual vehicles. Since the speed error and acceleration are the main factors affecting system stability, and fuel consumption and NO_x emissions primarily serve as constraints on the control objectives, this section uses the speed error and acceleration terms from the cost function as the Lyapunov function to assess system stability. Therefore, the candidate Lyapunov function is formulated as:

$$V(v,a) = \frac{1}{2}(v - v_{\text{ref}})^2 + \frac{1}{2}a^2. \tag{29}$$

First, the function must be evaluated for positivity, i.e.,

$$\begin{cases} V(v,a) > 0 & v \neq v_{\text{ref}} \text{ or } a \neq 0 \\ V(v_{\text{ref}},a) = 0 & a = 0 \end{cases}. \tag{30}$$

The speed error term, $\frac{1}{2}(v - v_{\text{ref}})^2$, is a quadratic function and is zero when $v = v_{\text{ref}}$. When $v \neq v_{\text{ref}}$, this term is positive. Hence, the speed error term is positive. Similarly, the acceleration term $\frac{1}{2}a^2$ is also a quadratic function and is always positive. Therefore, $V(v,a)$ satisfies the positivity condition. The specific form of its derivative is:

$$\dot{V}(v,a) = (v_p - v) \cdot a + a \cdot \dot{a}, \tag{31}$$

When the system tends toward stability, i.e., $v \to v_{\text{ref}}$, the acceleration and its derivative approach are zero. Therefore, near the system's stable point, $\dot{V}(v,a) \leq 0$, meaning $\dot{V}(v,a)$ is negative, the system gradually stabilizes.

Remark: In the following section, the simulation results are provided to empirically validate the proposed distributed control approach. The simulations will evaluate the system's performance subject to various operational conditions, with a particular focus on the effects of speed error and acceleration on vehicle stability, fuel consumption, and NO_x emissions. These results will offer a comprehensive evaluation of the control strategy's efficacy in maintaining platoon stability, while adhering to the constraints of fuel efficiency and emission reduction. A comparative analysis between the simulation results and the theoretical predictions will be conducted to further corroborate the practical applicability and robustness of the proposed method.

4. Simulations and Discussion

To validate the effectiveness of the proposed distributed algorithm for integrated fuel consumption and NO_x emissions optimization, simulation experiments were designed and compared against a Proportional–Integral (PI) control method and an SQP-based optimization approach. The PI controller was selected as a benchmark due to its widespread use in real-world platoon control applications. It is well-regarded for its simplicity and effectiveness in maintaining vehicle spacing and speed. However, PI control cannot incorporate fuel consumption and NO_x emissions as objectives, which limits its ability to optimize energy and environmental performance. The SQP method, on the other hand, is a classical numerical iterative approach that is widely used for solving nonlinear optimization problems with constraints. It was chosen to benchmark the computational performance of the proposed method against a gradient-based algorithm, commonly employed in optimization tasks. However, SQP requires smooth, differentiable objective functions and struggles with the high computational complexity associated with increasing dimensionality, such as that introduced by long prediction horizons. This makes it less suitable for real-time vehicle platoon control.

In regard to the first set of simulations, the control strategy without integrated fuel consumption and NO_x emissions optimization was compared with the proposed optimization approach. The objective was to assess the improvements in fuel consumption and emissions, as well as the associated costs. The second set of simulations compared the proposed optimization method with existing numerical iterative methods, aiming to validate its effectiveness in reducing the computation time. The parameters used in this study are sourced from [32], which provides data derived from a commercial vehicle model developed using GT-Power 7.5 software, featuring a 6-cylinder, 11.6 L diesel engine. This model is widely acknowledged for its robustness and reliability in representing the typical characteristics of heavy-duty commercial vehicles. Additionally, the accuracy of the model's parameters has been thoroughly validated in previous research, confirming its suitability for the detailed simulation and analysis of vehicle dynamics and control studies. By leveraging these validated parameters, this study ensures the reliability and generalizability of the results presented. The main parameters of the vehicle model used in these simulations are shown in Table 2.

Table 2. Main parameters of the simulated vehicle model.

Parameter	Value	Unit
Vehicle mass	7000	Kg
Tire radius	0.6	m
Frontal area	7	m^2
Transmission efficiency	0.95	-
Rolling resistance Coefficient	0.011	-

It is important to note that all the simulations were conducted using MATLAB R2023a and the experiments were run on a personal computer equipped with an Intel i9-12700H processor and 16 GB of memory. Additionally, a fixed simulation step size of 0.01 s was used for all the simulations.

4.1. Evaluation of Vehicle Following Performance

Research on the optimization of the lead vehicle speed has garnered widespread attention. Therefore, in the first set of simulations, it is assumed that the lead vehicle's speed information and road gradient variations are known, as shown in Figure 5. Specifically, the lead vehicle's speed includes steady-state driving, acceleration, and deceleration phases, while the road gradient encompasses flat, uphill, and downhill conditions. At the 40 s mark, a sudden reduction in the lead vehicle's acceleration is introduced to simulate realistic scenarios involving abrupt speed changes due to communication challenges or unexpected driving conditions. These simulations evaluate the proposed method's ability to adapt to external variations effectively, demonstrating its robustness in dynamic conditions.

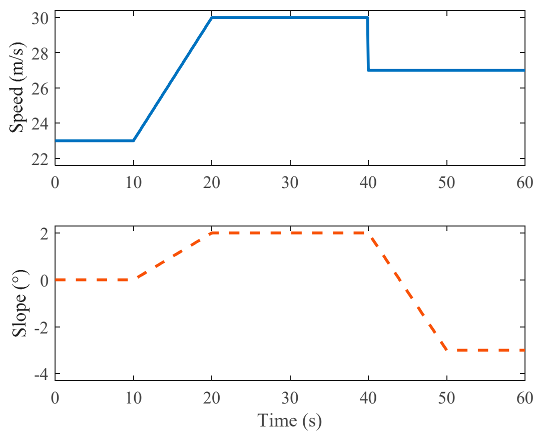

Figure 5. Leader vehicle speed and road slope.

In general, the vehicles in a platoon are affected in a similar manner. In this section, to validate the effectiveness of the control method when subject to different disturbances, it is assumed that the vehicles are subjected to different types of disturbances. The specific forms of these disturbances are shown in Figure 6. It is assumed that the second vehicle is subjected to a step-change disturbance caused by the tire conditions, which tests the controller's ability to handle abrupt changes in vehicle dynamics. The third vehicle is unaffected, serving as a baseline for comparison. The fourth vehicle experiences a steady disturbance caused by the road conditions, representing gradual but persistent environmental impacts. The fifth vehicle is subjected to random disturbances stemming from the engine combustion system and vehicle body structure, which simulate unpredictable and stochastic operating conditions. These disturbances are directly applied to the controller in the form of acceleration, making them a critical factor in evaluating its response to dynamic changes.

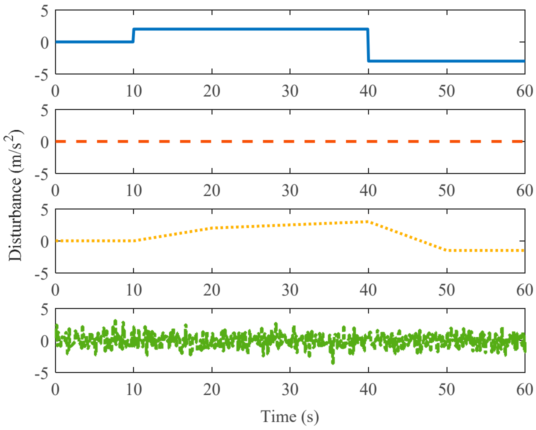

Figure 6. Disturbance form impacting different vehicles.

The choice of these distinct disturbance types directly impacts the evaluation of the proposed controller by offering a comprehensive assessment of its performance across multiple scenarios. A step-change disturbance measures the controller's responsiveness to abrupt variations, while a steady disturbance is used to assess its robustness in regard to sustained environmental factors. Additionally, a random disturbance evaluates the controller's capability to maintain stability amidst unpredictable and erratic influences. Collectively, these tests provide critical insights into the controller's effectiveness and suitability for real-world implementation, demonstrating its ability to ensure stable platoon operation in diverse and challenging conditions.

The initial vehicle spacing was set to 15 m. The stable operation of the platoon serves as the foundational basis for analyzing fuel consumption and NO_x emissions. As illustrated in Figure 7, the proposed method ensures stable platoon control in disturbance conditions, with the vehicle trajectories maintaining cohesion despite external disruptions. In comparison, Figure 8 shows the trajectory of the platoon in a disturbance-free scenario, where no significant differences in performance are observed. This indicates that the control strategy is robust enough to maintain stability and trajectory accuracy, even in the presence of disturbances, demonstrating the minimal impact of such disruptions on the overall platoon behavior.

As shown by the speed curve in Figure 9, the proposed controller effectively adjusts the vehicle speed in response to changes in the lead vehicle's speed. Even when the lead vehicle's speed fluctuates and the controlled vehicles are subjected to disturbances, the controller ensures that the speed of the vehicles within the platoon remains consistent, thereby maintaining platoon stability. Compared to the other vehicles in the platoon, the fifth vehicle exhibits a larger instantaneous speed deviation due to the random disturbance. However, this deviation does not propagate throughout the platoon, ensuring that the overall stability of the platoon is not compromised. This demonstrates the controller's robustness in handling disturbances, while maintaining cohesive and stable platoon dynamics.

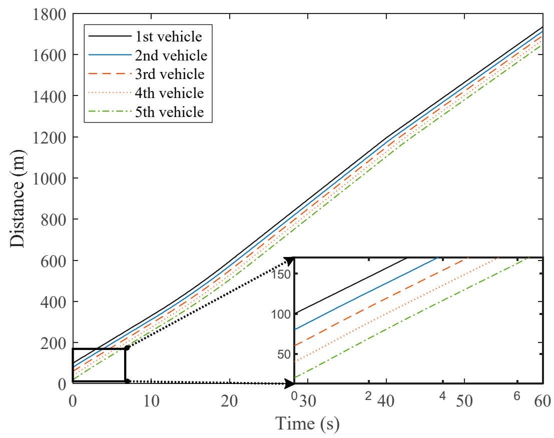

Figure 7. Platoon trajectory in disturbance conditions.

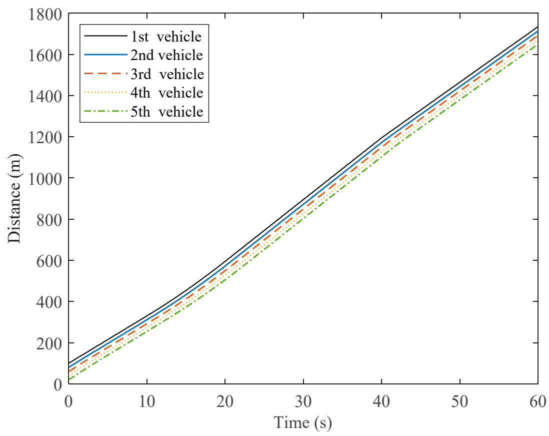

Figure 8. Platoon trajectory in disturbance-free conditions.

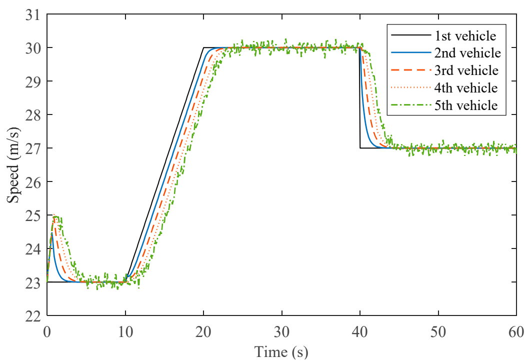

Figure 9. Vehicle speed in disturbance conditions.

In comparison, Figure 10 illustrates the vehicle speed without disturbances, where the platoon dynamics are smoother, yet the differences between the two conditions are minimal. This indicates that the controller demonstrates robustness. In the disturbance-free condition, the vehicle speed exhibits excellent smoothness in response to changes in both the road gradient and the lead vehicle speed. This smooth adaptation demonstrates the effectiveness of the proposed controller in maintaining stable speed profiles despite varying external conditions. The controller ensures the smooth operation of the platoon by reducing abrupt speed variations and promoting a consistent driving experience, even in the presence of external factors, such as changes in the road gradient or fluctuations in the lead vehicle's speed. This demonstrates the controller's ability to maintain stability and enhance the overall performance of the platoon.

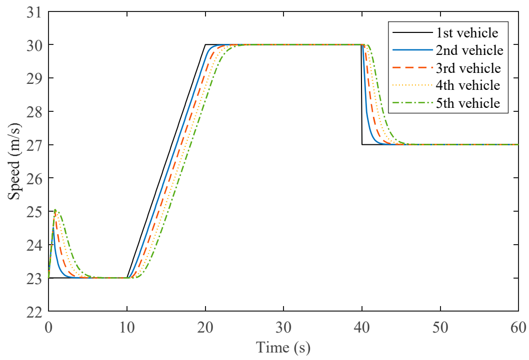

Figure 10. Vehicle speed in disturbance-free conditions.

As shown in Figure 11, the proposed controller regulates vehicle operation with minimal acceleration changes, thereby reducing the fuel consumption and NO_x emissions associated with rapid acceleration. Even when the vehicle is subjected to disturbances, the output acceleration tends to stabilize as the speed of the preceding vehicle remains constant. This ability to maintain stable acceleration helps to mitigate the negative impact of abrupt speed changes on fuel efficiency and emissions, further highlighting the controller's effectiveness in optimizing vehicle performance in varying conditions.

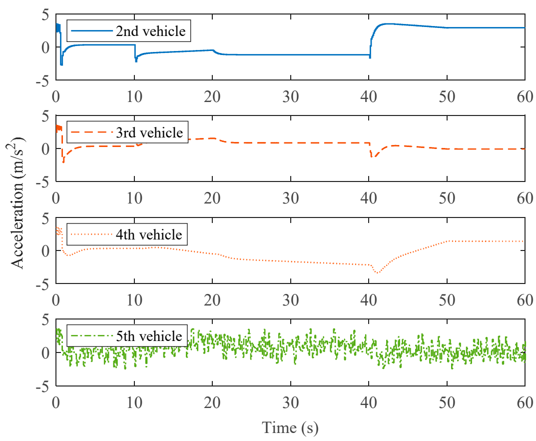

Figure 11. Vehicle acceleration curve.

4.2. Fuel Consumption and NO_x Emission Performance Analysis

Disturbances make it challenging to accurately analyze the fuel consumption and NO_x emissions of the following vehicles in relation to the lead vehicle. In regard to disturbance-free conditions, the instantaneous fuel consumption and NO_x emissions of the platoon are shown in Figures 12 and 13, respectively. Additionally, the average instantaneous fuel consumption and NO_x emissions over the simulation period are presented in Figure 14.

In the vehicle platoon, the vehicles positioned closer to the lead vehicle are directly influenced by its behavior. While they benefit from aerodynamic effects that help reduce fuel consumption and NO_x emissions, they are also more susceptible to disturbances caused by changes in the lead vehicle's speed. This is particularly noticeable during rapid acceleration or deceleration by the lead vehicle, which forces the following vehicles to react quickly, often compromising the efficiency of the optimization strategy. As a result, the optimization effects are less pronounced for these front vehicles compared to those further back in the platoon. Vehicles further back in the platoon benefit from both aerodynamic effects and a more stable speed profile. While the aerodynamic advantage reduces air resistance for trailing vehicles, contributing to lower fuel consumption and emissions, the primary factor is the optimized control strategy. This strategy, through APSO and DMPC, reduces the propagation of disturbances from the lead vehicle, allowing the trailing vehicles to experience fewer abrupt speed changes. As a result, these vehicles can operate more efficiently, with smoother acceleration and deceleration patterns, which further reduces fuel consumption and NO_x emissions compared to the lead vehicle. Thus, the combined effects of aerodynamic drag reduction and optimized speed control lead to significant efficiency improvements for the entire platoon.

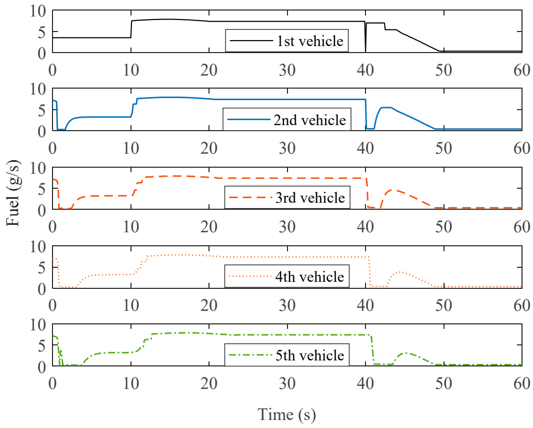

Figure 12. Instantaneous fuel consumption curve.

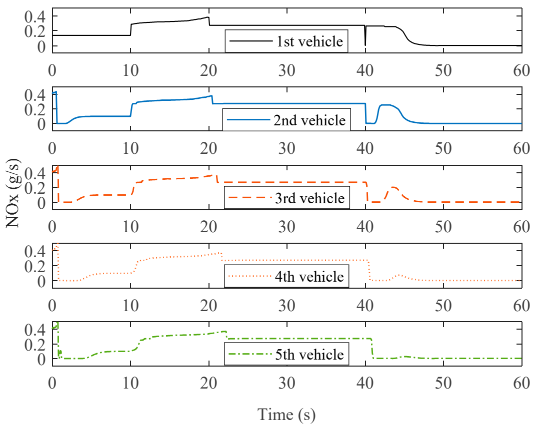

Figure 13. Instantaneous NO_x emission curve.

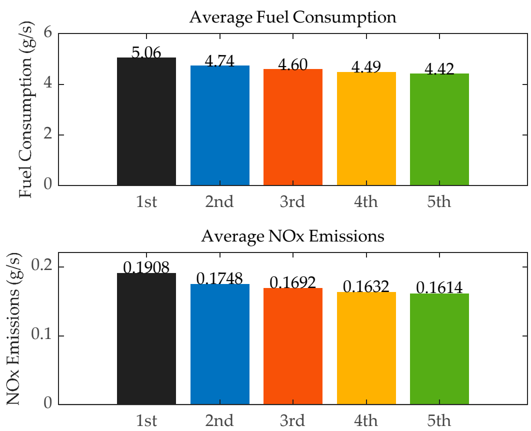

Figure 14. Average fuel consumption and NO_x emissions of platoon vehicles.

As shown in Table 3, the APSO controller enables vehicles within the platoon to reduce their fuel consumption and NO_x emissions to varying degrees compared to the lead vehicle.

Table 3. Comparative analysis of fuel consumption and NOx emissions for platoon vehicles.

Vehicle	Fuel (g/s)	Analysis	NO_x (g/s)	Analysis
1st	303.50	-	11.44	-
2nd	283.55	↓ 6.57%	10.45	↓ 8.65%
3rd	275.45	↓ 9.24%	10.11	↓ 11.63%
4th	268.81	↓ 11.43%	9.75	↓ 14.77%
5th	264.43	↓ 12.87%	9.64	↓ 15.73%

Since the reduction in aerodynamic drag within the platoon naturally contributes to lower fuel consumption and emissions for the following vehicles, it is important to evaluate the additional improvements achieved through the optimization provided by the proposed APSO controller. In this study, the PI control method is used as a baseline for comparison. Unlike the PI controller, which primarily focuses on maintaining platoon stability, the APSO controller incorporates fuel consumption and NO_x emissions optimization into the vehicle control strategy.

Figures 15 and 16 show comparisons between the overall fuel consumption and NO_x emissions of the two approaches for the entire platoon. The results indicate that, when the lead vehicle's speed varies, the overall fuel consumption and emissions of the platoon are better optimized by the APSO controller compared to the PI controller. This demonstrates that the APSO controller achieves improved fuel consumption and emissions performance, while maintaining stable operation of the platoon.

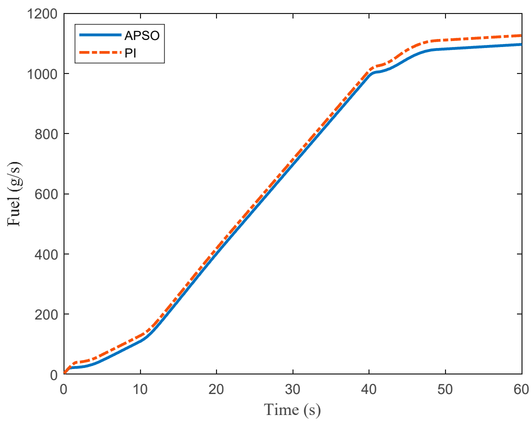

Figure 15. Platoon fuel consumption comparison.

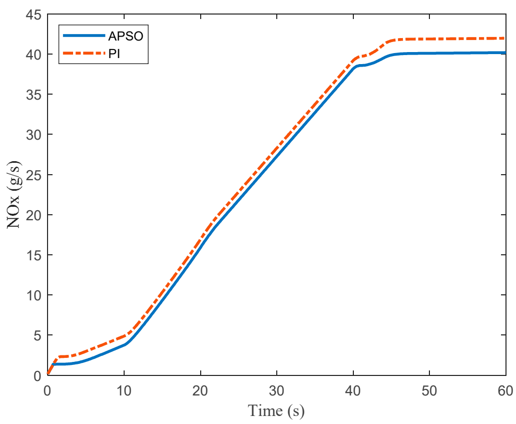

Figure 16. Platoon NO_x emissions comparison.

Tables 4 and 5 present detailed analyses comparing individual vehicle fuel consumption and NO_x emissions within the platoon. Figure 17 visually illustrates these comparisons, highlighting the advantages of the APSO controller over the PI controller. The results clearly demonstrate that, in addition to benefiting from reduced aerodynamic drag, the APSO controller further optimizes fuel consumption and NO_x emissions compared to the PI controller, thereby achieving better overall performance in regard to both environmental and control metrics.

Table 4. Fuel consumption comparison by vehicles within the platoon.

Vehicle	APSO Controller	PI Controller	Analysis
2nd	283.55	286.53	↓ 1.04%
3rd	275.45	282.16	↓ 2.38%
4th	268.81	278.34	↓ 3.42%
5th	264.43	274.90	↓ 3.81%

Table 5. NO_x emissions comparison from vehicles within the platoon.

Vehicle	APSO Controller	PI Controller	Analysis
2nd	10.45	10.67	↓ 2.06%
3rd	10.11	10.51	↓ 3.81%
4th	9.75	10.36	↓ 5.88%
5th	9.64	10.18	↓ 5.30%

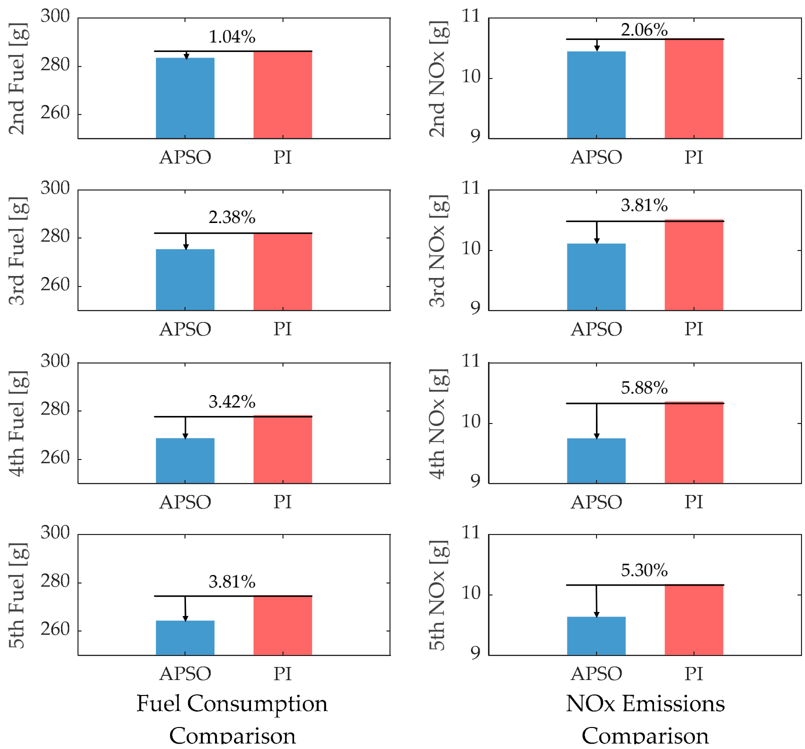

Figure 17. Comparative optimization analysis of APSO and PI controllers.

4.3. Timeliness Performance Analysis

A comparison with the commonly used numerical method, Sequential Quadratic Programming (SQP), was conducted to evaluate the computational efficiency of the APSO controller. First, using the same prediction step size, the control performance and computation time of the APSO method subject to the event-triggered mechanism were compared with those of the SQP method, with a 60 s simulation conducted using a time step of 0.01 s.

Next, the effect of the event-triggered mechanism on reducing computational events was analyzed. The results are illustrated in Figure 18.

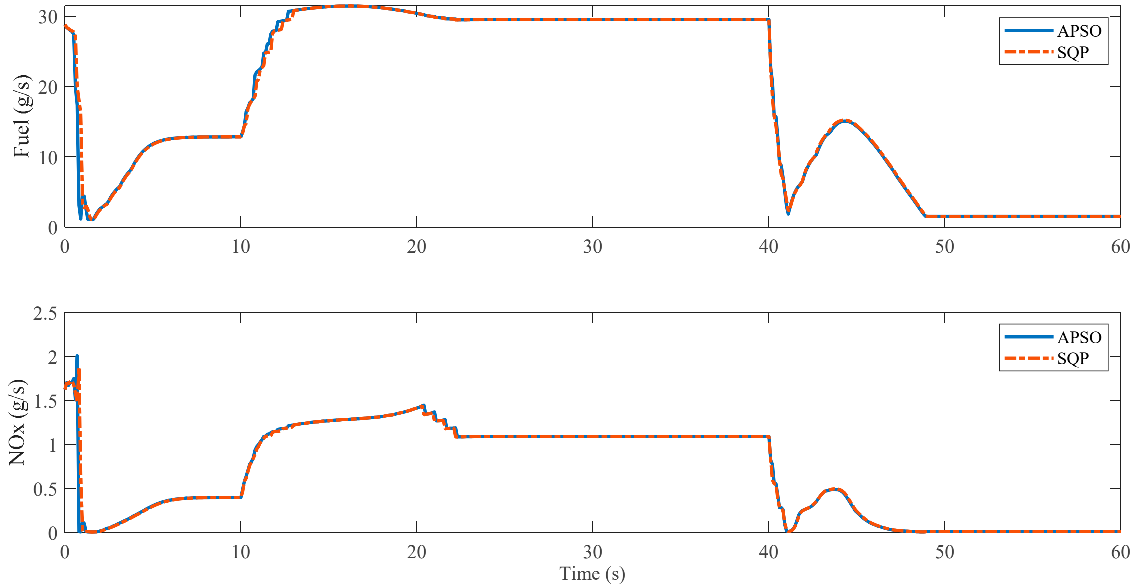

Figure 18. Instantaneous fuel consumption and NO_x emissions comparison of the platoon.

It can be observed that both methods achieve comparable results in terms of fuel consumption and emissions. Based on this, the computation times of the two methods are compared to analyze the impact of incorporating the event-triggered mechanism on computation efficiency. The total computation time statistics are shown in Table 6, which demonstrates that the method proposed in this study significantly reduces the overall runtime.

Table 6. Computation time of different methods.

Method	Time(s)	Analysis
Event-triggered APSO	4.81	↓ 77.96%
APSO	7.84	↓ 64.09%
Event-triggered SQP	12.08	↓ 44.66%
SQP	21.83	-

The APSO algorithm reduces the time required for iterative computations, while the introduction of the event-triggered mechanism further decreases the number of optimization calculations. This combination not only saves computational resources in regard to the vehicle itself, but also in regard to roadside units (RSUs), enhancing the overall efficiency in regard to resource utilization.

5. Conclusions

This paper studies energy-efficient driving strategies for intelligent connected commercial vehicle platoons on highways. A hierarchical optimization control strategy is proposed, consisting of upper-layer speed planning and lower-layer following control, to achieve coordinated control of fuel consumption and NO_x emissions across the platoon. The upper layer reduces system complexity by converting state constraints into reference speeds for vehicles. In the lower layer, a DMPC controller with APSO in event-triggered conditions is designed to effectively solve the nonlinear multi-objective optimization problem.

Simulation experiments validate the effectiveness of the proposed method, showing an 8.05% reduction in fuel consumption and a 10.15% reduction in NO_x emissions compared to the PI control strategy. Additionally, the computational speed improved by 77.9%

compared to numerical iterative methods, highlighting the efficiency of the proposed method in saving computational resources.

The results demonstrate that the proposed controller effectively reduces fuel consumption and NO_x emissions, while ensuring the stable operation of the platoon. Moreover, it significantly outperforms traditional numerical methods in terms of computational efficiency, highlighting its potential to optimize both energy usage and environmental performance across vehicle platoons.

Future efforts could focus on extending the control strategy to more complex driving scenarios and diverse vehicle types, including considerations involving tire friction, heterogeneous platoons, and controller design in extreme conditions. Additionally, conducting real-world tests, accounting for communication delays, and improving scalability for larger platoons would further enhance its practical applicability.

Author Contributions: Conceptualization, J.W. and Q.W.; methodology, J.W.; software, L.L.; validation, L.L.; writing—original draft preparation, L.L.; writing—review and editing, J.W.; visualization, L.L.; supervision, K.L. and Q.W.; project administration, J.L. All authors have read and agreed to the published version of the manuscript.

Funding: This research was funded by the Major Science and Technology Projects in Guangxi (AA24206054, AA24206047, AA22068064, AA22068066), the National Natural Science Foundation of China (61963006), the National Science Foundation of Guangxi Province (2018GXNSFAA050029, 2018GXNSFAA294085), and the Guangxi Key Laboratory of Automobile Components and Vehicle Technology (2022GKLACVTZZ01).

Institutional Review Board Statement: Not applicable.

Informed Consent Statement: Not applicable.

Data Availability Statement: The original contributions presented in the study are included in the article, further inquiries can be directed to the corresponding authors.

Conflicts of Interest: The authors declare that there are no conflicts of interest.

References

1. Li, Y.; Chen, W.; Peeta, S.; Wang, Y. Platoon control of connected multi-vehicle systems under V2X communications: Design and experiments. *IEEE Trans. Intell. Transp. Syst.* **2019**, *21*, 1891–1902. [CrossRef]
2. Liu, W.; Qin, G.; He, Y.; Jiang, F. Distributed cooperative reinforcement learning-based traffic signal control that integrates V2X networks' dynamic clustering. *IEEE Trans. Veh. Technol.* **2017**, *66*, 8667–8681. [CrossRef]
3. Li, S.E.; Zheng, Y.; Li, K.; Wu, Y.; Hedrick, J.K.; Gao, F.; Zhang, H. Dynamical modeling and distributed control of connected and automated vehicles: Challenges and opportunities. *IEEE Intell. Transp. Syst. Mag.* **2017**, *9*, 46–58. [CrossRef]
4. Zheng, Y.N. Time-varying formation control for unmanned intelligent vehicle (UIV) with mobile reference center. In Proceedings of the 2021 Asia-Pacific Conference on Image Processing, Electronics and Computers, Dalian, China, 14–16 April 2021; p. 042064.
5. Jond, H.B.; Yıldız, A. Connected and automated vehicle platoon formation control via differential games. *IET Intell. Transp. Syst.* **2023**, *17*, 312–326. [CrossRef]
6. Wang, P.; Chen, Z.; Zhang, X.; Ge, S.S. Space-and-time-synchronized simultaneous fully-actuated vehicle tracking/formation using cascaded prescribed-time control. *Int. J. Robust Nonlinear Control* **2022**, *32*, 2380–2398. [CrossRef]
7. He, D.; Qiu, T.; Luo, R. Fuel efficiency-oriented platooning control of connected nonlinear vehicles: A distributed economic MPC approach. *Asian J. Control* **2020**, *22*, 1628–1638. [CrossRef]
8. Mihaly, A.; Farkas, Z.; Gaspar, P. Model predictive coordination of autonomous vehicles crossing intersections. In Proceedings of the 21st IFAC World Congress, Berlin, Germany, 12–17 July 2020; Volume 53, pp. 15174–15179.
9. Li, S.; Chu, L.; Fu, P.; Pu, S.; Wang, Y.; Li, J.; Guo, Z. Energy-Oriented Hybrid Cooperative Adaptive Cruise Control for Fuel Cell Electric Vehicle Platoons. *Sensors* **2024**, *24*, 5065. [CrossRef] [PubMed]
10. Wen, S.; Guo, G. Control of leader-following vehicle platoons with varied communication range. *IEEE Trans. Intell. Veh.* **2019**, *5*, 240–250. [CrossRef]
11. Zhang, X.M.; Han, Q.L.; Zhang, B.L.; Ge, X.; Zhang, D. Accumulated-state-error-based event-triggered sampling scheme and its application to H∞ control of sampled-data systems. *Sci. China Inf. Sci.* **2024**, *67*, 162206. [CrossRef]
12. Zhang, X.M.; Han, Q.L.; Ge, X.; Zhang, B.L. Accumulative-error-based event-triggered control for discrete-time linear systems: A discrete-time looped functional method. *IEEE/CAA J. Autom. Sin.* **2024**, *11*, 1–11. [CrossRef]
13. Kazemy, A.; Lam, J.; Zhang, X.M. Event-triggered output feedback synchronization of master–slave neural networks under deception attacks. *IEEE Trans. Neural Netw. Learn. Syst.* **2020**, *33*, 952–961. [CrossRef]

14. Wen, S.; Guo, G.; Chen, B.; Gao, X. Cooperative adaptive cruise control of vehicles using a resource-efficient communication mechanism. *IEEE Trans. Intell. Veh.* **2018**, *4*, 127–140. [CrossRef]
15. He, B.; Gao, F. Influence analysis of leader information with application to formation control of multi-agent systems. *Int. J. Control Autom. Syst.* **2020**, *18*, 3062–3072. [CrossRef]
16. Hu, J.; Bhowmick, P.; Arvin, F.; Lanzon, A.; Lennox, B. Cooperative control of heterogeneous connected vehicle platoons: An adaptive leader-following approach. *IEEE Robot. Autom. Lett.* **2020**, *5*, 977–984. [CrossRef]
17. Wen, J.; Wang, C.; Xu, P.; Xie, G. Decentralized event-triggered circle formation control for multiagent systems via synchronous periodic event detection. *Int. J. Robust Nonlinear Control* **2020**, *30*, 910–925. [CrossRef]
18. Massera Filho, C.; Terra, M.H.; Wolf, D.F. Safe optimization of highway traffic with robust model predictive control-based cooperative adaptive cruise control. *IEEE Trans. Intell. Transp. Syst.* **2017**, *18*, 3193–3203. [CrossRef]
19. Guo, X.G.; Wang, J.L.; Liao, F.; Teo, R.S.H. CNN-based distributed adaptive control for vehicle-following platoon with input saturation. *IEEE Trans. Intell. Transp. Syst.* **2017**, *19*, 3121–3132. [CrossRef]
20. Zhu, P.; Jin, S.; Bu, X.; Hou, Z. Distributed Data-Driven Event-Triggered Fault-Tolerant Control for a Connected Heterogeneous Vehicle Platoon With Sensor Faults. *IEEE Trans. Intell. Transp. Syst.* **2023**, *25*, 5498–5509. [CrossRef]
21. Feng, G.; Dang, D.; He, Y. Robust coordinated control of nonlinear heterogeneous platoon interacted by uncertain topology. *IEEE Trans. Intell. Transp. Syst.* **2020**, *23*, 4982–4992. [CrossRef]
22. Gao, Z.; Guo, G. Command-filtered fixed-time trajectory tracking control of surface vehicles based on a disturbance observer. *Int. J. Robust Nonlinear Control* **2019**, *29*, 4348–4365. [CrossRef]
23. Liu, W.; Wei, Z.; Liu, Y.; Gao, Z. Adaptive Fixed-Time Safety Concurrent Control of Vehicular Platoons with Time-Varying Actuator Faults under Distance Constraints. *Mathematics* **2024**, *12*, 2560. [CrossRef]
24. Santini, S.; Albarella, N.; Arricale, V.M.; Brancati, R.; Sakhnevych, A. On-board road friction estimation technique for autonomous driving vehicle-following maneuvers. *Appl. Sci.* **2021**, *11*, 2197. [CrossRef]
25. Zuo, L.; Wang, P.; Yan, M.; Zhu, X. Platoon tracking control with road-friction based spacing policy for nonlinear vehicles. *IEEE Trans. Intell. Transp. Syst.* **2022**, *23*, 20810–20819. [CrossRef]
26. Wang, J.; Lian, Y.; Jiang, Y.; Xu, Q.; Li, K.; Jones, C. Distributed data-driven predictive control for cooperatively smoothing mixed traffic flow. *Transp. Res. Part C Emerg. Technol.* **2023**, *155*, 104274. [CrossRef]
27. Ma, Y.; Liu, Q.; Fu, J.; Liufu, K.; Li, Q. Collision-avoidance lane change control method for enhancing safety for connected vehicle platoon in mixed traffic environment. *Accid. Anal. Prev.* **2023**, *184*, 106999. [CrossRef]
28. Huang, C.; Shi, Q.; Ding, W.; Mei, P.; Karimi, H.R. A robust MPC approach for platooning control of automated vehicles with constraints on acceleration. *Control Eng. Pract.* **2023**, *139*, 105648. [CrossRef]
29. Qiu, M.; Liu, D.; Baldi, S.; Yin, G.; Yu, W.; Cao, M. Vehicular platooning on curved paths considering collision avoidance and string stability. *IEEE Trans. Netw. Sci. Eng.* **2023**, *11*, 1896–1908. [CrossRef]
30. Min, H.; Yang, Y.; Fang, Y.; Sun, P.; Zhao, X. Constrained optimization and distributed model predictive control-based merging strategies for adjacent connected autonomous vehicle platoons. *IEEE Access* **2019**, *7*, 163085–163096. [CrossRef]
31. Shi, J.; Li, K.; Chen, C.; Kong, W.; Luo, Y. Cooperative merging strategy in mixed traffic based on optimal final-state phase diagram with flexible highway merging points. *IEEE Trans. Intell. Transp. Syst.* **2023**, *24*, 11185–11197. [CrossRef]
32. Liu, D.; Chen, H.; Sun, Y.; Hu, Y. Heavy-duty diesel vehicle formation with transient integrated control of fuel consumption and emission in an intelligent network environment. *Proc. Inst. Mech. Eng. Part I J. Syst. Control Eng.* **2022**, *236*, 1830–1844. [CrossRef]
33. Kamal, M.A.S.; Mukai, M.; Murata, J.; Kawabe, T. Ecological driving based on preceding vehicle prediction using MPC. *IFAC Proc. Vol.* **2011**, *44*, 3843–3848. [CrossRef]
34. Kamal, M.A.S.; Mukai, M.; Murata, J.; Kawabe, T. Model predictive control of vehicles on urban roads for improved fuel economy. *IEEE Trans. Control Syst. Technol.* **2012**, *21*, 831–841. [CrossRef]
35. Chen, H.; Guo, L.; Ding, H.; Li, Y.; Gao, B. Real-time predictive cruise control for eco-driving taking into account traffic constraints. *IEEE Trans. Intell. Transp. Syst.* **2018**, *20*, 2858–2868. [CrossRef]
36. Earnhardt, C.; Groelke, B.; Borek, J.; Vermillion, C. Hierarchical model predictive control approaches for strategic platoon engagement of heavy-duty trucks. *IEEE Trans. Intell. Transp. Syst.* **2021**, *23*, 8234–8246. [CrossRef]
37. Nie, Z.; Zhu, L.; Jia, Y.; Lian, Y.; Yang, W. Hierarchical optimization control strategy for intelligent fuel cell hybrid electric vehicles platoon in complex operation conditions. *Int. J. Hydrogen Energy* **2024**, *50*, 1056–1068. [CrossRef]
38. Yao, Z.; Wang, Y.; Liu, B.; Zhao, B.; Jiang, Y. Fuel consumption and transportation emissions evaluation of mixed traffic flow with connected automated vehicles and human-driven vehicles on expressway. *Energy* **2021**, *230*, 120766. [CrossRef]
39. Guo, L.; Sun, M.; Hu, Y.; Chen, H. Optimization of fuel economy and emissions through coordinated energy management for connected diesel vehicles. *IEEE Trans. Intell. Veh.* **2023**, *8*, 3593–3604. [CrossRef]